Asian Journal of Physics
Vol. 33, Nos 1 & 2 (2024) 1-14
Available on: www.asianjournalofphysics.com

ap

Cellular lipid droplets observed in absorption, emission, and scattering - potential and limitations of various spectroscopic methods

Anna M Nowakowska[1], Patrycja Dawiec[1,2], Karolina Chrabąszcz[3,1], Anna Pieczara[2,4], Krzysztof Brzozowski[1], Mariusz Kępczyński[1], and Katarzyna Majzner[1]

[1]*Department of Chemical Physics, Faculty of Chemistry, Jagiellonian University, Gronostajowa 2, 30-387 Krakow, Poland*

[2]*Doctoral School of Exact and Natural Sciences, Jagiellonian University, Lojasiewicza 11, 30-348 Krakow, Poland*

[3]*The Henryk Niewodniczanski Institute of Nuclear Physics, Polish Academy of Sciences, Radzikowskiego 152, 31-342 Krakow, Poland*

[4]*Jagiellonian Centre for Experimental Therapeutics, Jagiellonian University, Bobrzynskiego 14, 30-348 Krakow, Poland*

Lipids are a primary source of long-term energy storage and essential in constructing cellular membranes. They also play an important role as mediators in signaling. At the subcellular level, lipids are stored in specialized structures known as lipid droplets (LDs). These droplets serve as dynamic organelles involved in lipid metabolism. LDs can be found in many types of cells, but their number, size, and composition vary greatly and depend on the type, metabolism, and condition of cells.

Tracking LDs in cells provides insights into lipid metabolism, and their presence is frequently linked to the development of diseases. Various imaging techniques, with fluorescence microscopy playing a leading role, are employed for their observation. Although, it allows sensitive detection of LDs in cells, it does not provide insight into their chemical structure. Its limitations include photobleaching and the limited number of dyes that can be detected simultaneously. For this reason, new methods are still being sought to provide better insight into LDs' molecular structure and function. Among a group of techniques that provide insight into the composition of LDs are spectroscopic methods, such as infrared and Raman imaging.

In our investigation, we performed a multiparameter spectroscopic analysis of LDs in single endothelial and leukemic cells, comparing the results with classical fluorescence staining. Cells were incubated with an exogenous fatty acid, deuterated palmitic acid, to monitor the *de novo* formation of LDs. We employed three distinct spectroscopic techniques: infrared spectroscopy, spontaneous Raman imaging, and Stimulated Raman Spectroscopy, which were used to verify their efficacy in analyzing LDs in endothelial and leukemic cells. Our findings demonstrate the suitability of these techniques for tracing the chemical composition of LDs, enabling differentiation between newly formed LDs resulting from fatty acid uptake and endogenous lipids within the cell. Additionally, we highlight the advantages and limitations of spectroscopic techniques for studying LDs in individual cells, facilitating the selection of an appropriate tool for investigating lipid metabolism.

Keywords: Lipid droplets, Raman imaging, SRS, Fluorescence, Endothelium, Leukemia, Deuterated palmitic acid.

1 Introduction

Lipids, particularly triacylglycerols, play a crucial role in the energy storage of cells. Due to their amphiphilic nature, triacylglycerols and cholesterol esters act as building blocks of cell membranes and

Corresponding authors
e mail:katarzyna.b.majzner@uj.edu.pl (Katarzyna Majzner)

serve as a secondary messengers or regulators in cellular signal transduction and transport [1]. *In vitro,* stored lipids can be found in specific structures known as lipid droplets (LDs). LDs are dynamic organelles present in numerous cell types, displaying diversity in numbers, sizes, and compositions. They play a pivotal role in maintaining lipid homeostasis, a critical process for constructing cellular membranes and the functioning of signaling pathways. LDs are characterized by a high lipid content, particularly enriched in fatty acids [2], and are surrounded by a phospholipid monolayer [2]. LDs are also known for their regulatory function in eosinophils, neutrophils, and tumor cells [3]. Most animal cells accumulate lipids for a short period, depending on their ages, physiological state, and the conditions under which they grow. Some cells can induce lipid storage under stress, inflammation, or disease [4–8] and other inflammatory conditions. Here, we will review the contemporary evidence related to the biogenesis and structure of leukocyte lipid bodies (also known as lipid droplets). The distinctive location of LDs is within specialized regions of the endoplasmic reticulum. Additionally, a specific surface-bound protein associated with LDs, such as perilipins and adipose differentiation-related protein (ADRP), has been identified in these areas [9]. LDs are crucial in the pathogenesis associated with metabolic diseases such as diabetes, obesity, and atherosclerosis. Various studies have highlighted the diversity of LDs and their interactions with other organelles in cells [10].

In forming LDs, coenzyme A (CoA) plays a crucial role, particularly in activating fatty acids. The process involves the conversion of fatty acids into acyl-CoA, which is a precursor for the synthesis of triglycerides, a significant component of LDs. The formation of LD begins within the endoplasmic reticulum (ER), where fatty acids are esterified to glycerol-3-phosphate, forming triglycerides. Sterol esters, another type of lipid, can also contribute to forming LDs. As triglycerides and sterol esters accumulate, small LDs buds from the ER membrane. These droplets continue to grow as more lipids are incorporated into their core [6-10].

LDs formed through the accumulation of neutral lipids, primarily triglycerides and sterol esters, within the endoplasmic reticulum (ER), are coated with proteins, such as perilipins, helping to regulate LDs size and stability. These coated LDs can then be transported to various cellular locations. Lipases come into play when the cell needs energy or lipids for membrane synthesis. Lipases are enzymes responsible for breaking down triglycerides into fatty acids and glycerol. Under lipolysis, LDs can undergo fission, a process in which a single large LD splits into multiple smaller LDs. Fission corresponds to a drastic increase in the surface area of LDs, providing more access points for lipases to act on [10]. There are also many proofs that LDs are active organelles that interact with other cellular substructures organelles, particularly mitochondria, endosomes, ER, plasma membrane, and peroxisomes [2,11]. Some hypotheses suggest that LDs may serve as a protective reservoir for unfolded proteins, potentially preventing detrimental interactions with other cellular components. This idea suggests that LDs, known for storing lipids, may also play a role in sequestering unfolded or misfolded proteins. This process could help maintain cellular balance by reducing the potential harm caused by unfolded proteins. However, the exact mechanisms and extent of the involvement of LDs in this process are still being studied [12].

Various imaging techniques are used to understand the functions and properties of lipids and LDs in cells. Among these techniques, fluorescence microscopy is the most widely used. It involves using a dye with a chromophore group in its structure that explicitly binds to lipids [13-16]. The most common dyes used to visualize such organelles are Nile Red, LipidTox, and BODIPY 493/503 [17]. Since LDs differ in many types of cells, this aspect must have been considered when choosing the dyes [18,19]. Furthermore, the preparation of cells, including fixation methods, must be deliberate [17,20]. Fluorescence measurements provide helpful information on the presence of LDs in cells. They can provide information about changes in the number and size of LDs under the influence of some agents or inflammation [21]. The advantage of fluorescence microscopy is also short time of measurements. Images of many cells can be obtained in one rapid scan, since the field of view is much larger than in conventional bright-field microscopy [22].

In contemporary research, there is a search for sample-preparation-free methods that offer expedited analyses. In contrast to fluorescence, vibrational spectroscopic techniques, like infrared (IR) or Raman spectroscopic methods, stand out due to their independence from dyes, non-invasiveness, and ability to furnish details about LDs' chemical composition and structure. Although infrared spectroscopy is commonly employed for protein examination, there are notable instances where this technique has been successfully applied to investigate LDs in intact oleaginous yeasts [23] or in atherosclerotic arteries [24]. Considering the high cross-section for scattering in lipids, Raman seems to be a method of choice for studies of long non-polar acyl chains [25]. Compared to IR, Raman spectroscopy enables imaging with a higher spatial resolution due to excitation wavelengths [26], but it is often hindered by low sensitivity. Moreover, the combination of confocal microscopy with Raman spectroscopy, called Confocal Raman Microscopy, enables 3D imaging of cells (fixed or alive) and visualization of LDs in the entire volume of cells [27-31]. Raman imaging provides morphological (size, number) and molecular information about LDs. Spontaneous Raman imaging with high spatial resolution is time-consuming; therefore, nowadays, rapid Raman methods are developed to examine LDs, such as Stimulated Raman Spectroscopy (SRS) or Coherent Anti-Stokes Raman Scattering (CARS) [32-35]. Rapid methods have great diagnostic potential in the analysis of lipids. LDs may become a universal Raman marker of inflammation, enabling the testing of new anti-inflammatory drugs in the model systems.

Our study aimed to compare various spectroscopic methods, such as infrared spectroscopy, spontaneous Raman imaging, and Stimulated Raman Spectroscopy, to visualize the formation of LDs resulting from the uptake of deuterated palmitic acid (PA-d_{31}) in endothelial and leukemic cells. We compared vibrational spectroscopic imaging with a gold-standard method for studying cellular composition, fluorescent imaging. Our results show that Raman and infrared spectroscopic imaging offers distinct advantages over fluorescent imaging, allowing visualization of subcellular component distribution and simultaneous analysis of the structure and composition of multiple biomolecules.

2 Methodology

Endothelial cells preparation

Two commercially available endothelial cell lines were used. Primary human microvascular endothelial cells (HMEC-1) were purchased from Gibco and cultured in a supplemented endothelial cell growth medium (MCDB 131; Gibco). Primary Human Aortic Endothelial Cells (HAECs) were purchased from Lonza and cultured in a supplemented endothelial cell growth medium (EGM-2MV; Lonza). Cells were incubated in a humidified cell culture incubator at 37 °C in 5% CO_2/ 95% air. The cells were grown directly on calcium fluoride windows (CaF_2, 25×2 mm, Crystan Optics, UK) for all spectroscopic measurements, which were placed in 6-well plates. Cells were seeded at a number of 150,000 per well. HMEC-1 cells from passage 3 were incubated with 50 µM sodium salt of deuterium-labelled saturated palmitic acid (PA-d_{31}, Sigma Aldrich) conjugated to BSA (10%; Sigma-Aldrich) for 16 hours. HAEC cells were incubated with 200 µM sodium salt of PA-d_{31} conjugated to BSA for 18 h. Control cells were grown in a medium with the addition of sterile water and BSA. After incubation, cells were fixed for 4 min with 2.5 % glutaraldehyde and stored in isotonic phosphate buffer (PBS, Gibco), pH = 7 at 4 °C until data acquisition.

Leukemic cells preparation

Promyeloblastic HL-60 cells were purchased from Sigma Aldrich and cultured in a supplemented RPMI medium (10% FBS, 1% Antibiotic-Antimycotic, Gibco). Cells were incubated at 37 °C in a 5% CO_2/ 95% air humidified cell culture incubator. For experiments, 1 mln of cells was placed in a 6-well plate (0.3 mln/ml). The cells were then incubated with 200 µM PA-d_{31} sodium salt of PA-d_{31} (Sigma Aldrich) conjugated to BSA for 18 h (10%; Sigma-Aldrich) for 18 hours. Control cells were incubated with BSA. After incubation, cells were centrifuged (300g, 5 min), washed with PBS, and fixed with 0.5% glutaraldehyde

solution for 10 min. After fixation, cells were washed three times with PBS and stored at 4 °C. Right before measurement, HL-60 cells were deposited onto CaF_2 slides and measured after sedimentation and stabilization were completed.

Fluorescence measurements

After 16 h of exposure to PA-d_{31}, HMEC-1 endothelial cells were washed twice with PBS, fixed with 2.5 % glutaraldehyde *per* 4 minutes, blocked with BSA (1% BSA, 30 min), and counterstained for LDs with BODIPY 493/503 (Invitrogen Molecular Probes, 60 minutes) and with Hoechst 33342 (Life Technologies, 10 minutes) for nuclei. The fluorescence images were collected in DAPI and FITC channels (excited with 405 and 488 nm diode lasers) for the nucleus and LDs, respectively. 2D fluorescence images of cells with LDs were collected using the Olympus ScanR system, and 3D fluorescence images of PA-d_{31}-incubated cells were acquired with an A_1-Si Nikon (Japan) confocal laser scanning system built onto a Nikon inverted microscope Ti-E using a Plan Apo 100×/1.4 Oil DIC objective. Images were recorded at a resolution of 1024×1024.

To stain LDs and nuclei in leukemic cells, fixed HL-60 cells were centrifuged (300 g, 5 min, RT), washed with DPBS, and then simultaneously incubated with LipidTox (Invitrogen) and Hoechst 33342 (ThermoFisher). After 20 min, cells were centrifuged (300 g, 5 min, RT), washed with DPBS, and resuspended in 50 µl DPBS. Before measurement, 10 µl of the sample was placed onto a primary slide and covered with a coverslip. Cells were imaged in the DAPI and PI channels. The fluorescence measurements of HL-60 cells were taken using an optical microscope (Olympus CKX53, Olympus DP74, Tokyo, Japan) equipped with Olympus LCAch N 40× (NA = 0.55, iPC) objective (Olympus, Tokyo, Japan), high-resolution DP74 camera (Olympus, Tokyo, Japan) and CellSens software (Olympus, Tokyo, Japan). A high-brightness U-LGPS light source was used to excite fluorescence.

Infrared measurements

Shortly before the Fourier transform infrared spectroscopic (FTIR) measurements, the HAEC cells were washed gently with doubly deionized water to remove residual PBS from the surface of the cells and then left to air-dry. HL-60 cells are non-adherent cells; therefore, they were placed onto CaF_2 windows and air-dried. The experiments were performed using the Varian 620-IR microscope coupled to a 670-IR spectrometer with a 128×128 pixel focal plane array (FPA) detector with a spatial resolution of 5.5 µm per pixel in transmission mode. Measurements were performed with a 15× Cassegrain objective and condenser, collecting 256 and 128 co-scans for background and sample images, respectively (standard resolution). All spectra were recorded in the 3600-900 cm^{-1} region with a spectral resolution of 8 cm^{-1}. Infrared data were collected and initially analyzed with the use of Varian Resolutions Pro software (ver. 5.0.0.640) and CytoSpec software (ver. 2.00.01).

Spontaneous Raman measurements

Confocal Raman imaging measurements were performed using a WITec Confocal Raman Microscope (WITec alpha 300) with a 532 nm laser. The laser power was around 15 mW. The laser was coupled with an optical fiber (50 µm core diameter) to the spectrometer. Spectra of endothelial cells were collected using a 63× water immersion objective (Nikon Fluor, NA=1). The step size was equal to 0.5 µm, and the integration time was equal to 0.5 s *per* spectrum. HL-60 spectra were collected using a 40× water immersion objective (Zeiss W Plan-Apochromat VISIR, NA=1). The integration time was 0.1 s *per* spectrum. High-resolution (HR) imaging was performed for leukemic cells with a step size equal to 0.162 µm. Additionally, 3D imaging was performed with a step size equal to 0.5 µm (x, y-axis) or 1 µm (z-axis). The spectral resolution was 3 cm^{-1}.

Stimulated Raman Spectroscopy

Cells from two cell lines, HAEC and HL-60, were treated with 200 µM of PA-d_{31} for 18 h and measured using the homemade SRS setup. The system has a 2 ps laser (Fluence Lazurite, Fluence sp. z

o.o.) with a 20 MHz repetition rate. The system is based on a fiber laser producing a Stokes beam at 1029 nm with 450 mW of average power with a built-in optical parametric oscillator (OPO) that produces a tunable wavelength beam in the range of 750 - 950 nm with an average power of 100 mW that is used as the Pump beam. In our setup, the Stokes beam was modulated with an acousto-optic modulator (AOM), and the stimulated Raman loss (SRL) signal with 4MHz's modulation was collected. A 40× air objective (Olympus, NA=0.75) was used to focus overlapped Stokes and Pump beams on the sample. A 50× water dipping objective (Nikon, NA=1) collected the transmitted pump beam. The signal was retrieved using the Stanford Research Systems SR865A lock-in amplifier, sent to the electronics, and stored by Control FIVE 6.1 software (WITec GmbH). During measurements, the powers of Stokes and Pump beams before the sample were set to 25 and 12.5 mW, respectively. Imaging was performed with 25×25 μm^2 frames for HAEC cells and 40×30 μm^2 for HL-60 cells. The pixel dwell time was set to 900 µs in both cases. Images were collected at Pump beam values of 791.0 nm (2930 cm^{-1}, organic matter), 796.0 nm (2850 cm^{-1}, lipids), and 846.0 nm (2100 cm^{-1}, the C-D stretching).

3 Results and discussion

Fluorescent measurements

The gold standard method for tracking the formation of LDs with relatively high sensitivity in single cells is fluorescence microscopy [36,37]. Figure 1 shows LDs in PA-d_{31}-treated endothelial cells (Fig 1A-B) and HL-60 cells (Fig 1C). In the case of endothelial cells, LDs were stained using BODIPY 493/503, while LDs in leukemic cells were visualized using LipidTox. In both cell lines, incubation with PA-d_{31} significantly increased LDs formation, confirming PA-d_{31} uptake by endothelial and leukemic cells. The high magnification of the objectives (100× for endothelial cells and 40× for leukemic cells) allows visualization of even a single LD with high contrast and image quality (Fig 1B). Fluorescence image analysis cannot differentiate between newly formed LDs resulting from exogenous fatty acid uptake and those already present in cells under normal conditions. This is because fluorescence microscopy does not provide any information about the chemical composition of the LDs. As a result, monitoring biochemical changes related to lipid metabolism and understanding the fatty acid uptake process becomes challenging since LDs accumulated in cells beforehand cannot be distinguished from those formed by fatty acid uptake. What is more, additional information on accompanying metabolic changes related to proteins or nucleic acids cannot be obtained unless other cellular substructures are stained. Furthermore, in fluorescence microscopy, the number of fluorescent labels that can be used simultaneously is limited due to the broad emission spectra of the dyes [38]. For this reason, other metabolomics methods are being researched, enabling simultaneous real-time tracking of many biomolecules in living cells. Vibrational spectroscopic methods (infrared and Raman spectroscopy) respond to this need. Therefore, in this study, they were chosen to track fatty acid uptake and verify their use in the single-cell metabolism examination.

Infrared imaging

Infrared spectroscopy belongs to spectroscopic methods and, together with Raman spectroscopy, allows the study of the biochemical composition of cells and tissues [38-43]. According to the Rayleigh criterion, IR microscopy generally yields lower spatial resolution than Raman microscopy. However, IR spectroscopy allows for faster measurements of cells and larger tissue fragments compared to spontaneous Raman imaging. Figure 2 shows infrared images of PA-d_{31}-treated and control HAEC (Fig 2A) and HL-60 (Fig 2B) cells.

The first column of Figure 2 presents microphotographs of dried cells deposited onto the CaF_2 window. False-color images obtained using hierarchical cluster analysis (HCA) show the spatial distribution of the spectra from four defined clusters. The HCA results were complemented by integration maps showing

the spatial distribution of proteins (integration over the amide I band at 1650 cm^{-1}) and PA-d_{31} (integration over the C-D stretching band at 2100 cm^{-1}). To visualize the molecular changes accompanying the uptake and metabolism of PA-d_{31} into proteins, nucleic acids, and lipids, the infrared spectra of both PA-d_{31}-treated and control cells for endothelial and leukemic cells were compared. This approach provides important information on the spatial distribution of the major subcellular components

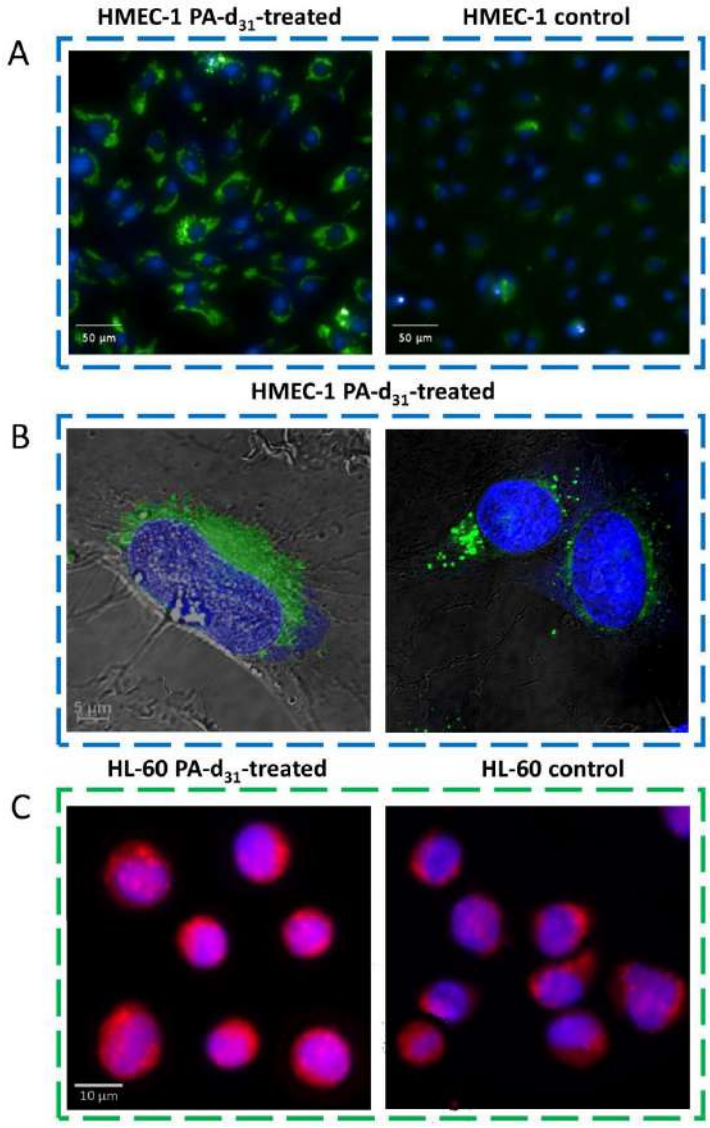

Fig 1. Fluorescence imaging of LDs in single endothelial and leukemic cells. LDs in HMEC-1 cells visualized using BODIPY 493/503 (A, B): images collected with a 20× objective and Olympus ScanR system (A): right-PA-d_{31}-incubated cells, left-control cells (scale bar: 50 µm), and images collected with the confocal laser scanning system A1-Si Nikon (Japan) at a magnification of 100× (B). LDs in HL-60 cells were visualized using LipidTox (C): right-PA-d_{31}-incubated cells and left-control cells (scale bar: 5 µm) collected using an inverted microscope Olympus CKX53 (Tokyo, Japan) at 40× magnification (scale bar: 10 µm).

of cells [44]. Analysis of the IR spectra reveals the presence of bands indicative of C-D vibrations at approximately 2190 cm^{-1} and 2090 cm^{-1} after PA-d_{31} incubation, confirming the uptake of fatty acids. The integration map further supports this observation, illustrating the spatial distribution of C-D vibrations in PA-d_{31}-treated cells. Additionally, distinct molecular changes are evident when comparing PA-d_{31}-treated cells (marked in red) with control cells (marked in blue), particularly in the fingerprint spectral range associated with proteins (alteration in the ratio of the amide I band at 1650 cm^{-1} and the amide II band at 1540 cm^{-1}) and nucleic acids (changes in band intensities at 1235 cm^{-1} and 1085 cm^{-1}).

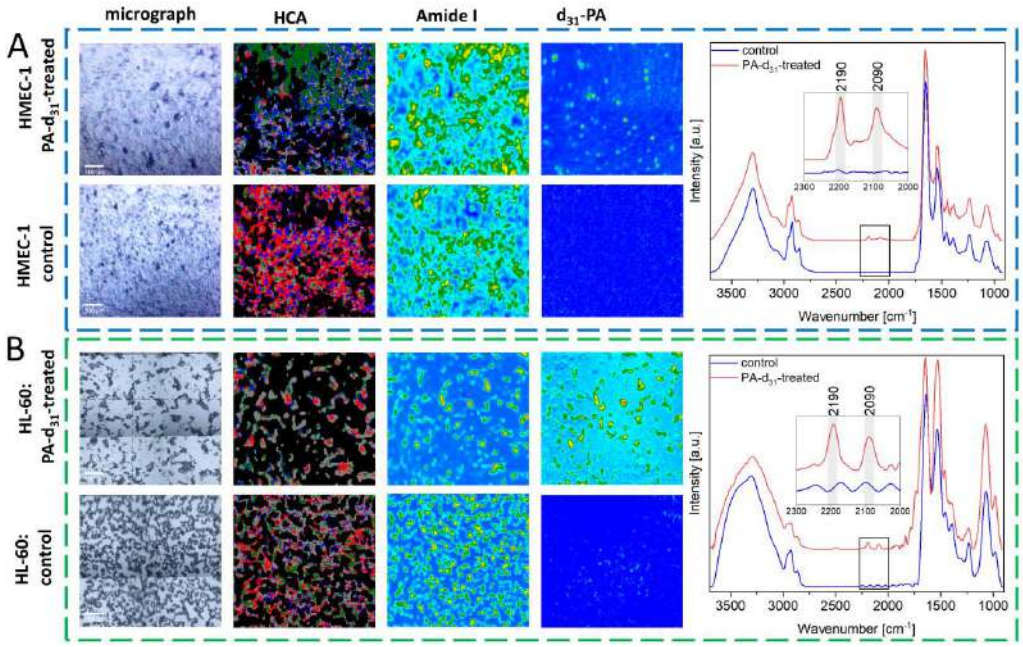

Fig 2. Infrared imaging of PA-d_{31}-treated and control HMEC-1 (A) and HL-60 (B) cells. Left panel: a microphotograph of dried cells and false-color HCA images; middle panel: protein distribution (IR image for the amide I band at 1650 cm^{-1}) and PA-d_{31} distribution (IR image for the C-D stretching band at 2100 cm^{-1}); and right panel: cellular spectra from the HCA analysis of control (blue) and PA-d_{31}-treated cells (red, scale bar: 100 μm).

The comprehensive analysis of the IR images and the corresponding spectra indicates that, despite exhibiting lower spatial resolution compared to fluorescence microscopy and Raman spectroscopy, IR imaging provides valuable insights into the chemical composition of cells and enables tracking metabolic changes induced by fatty acid uptake. However, it should be noted that at the single-cell level, IR imaging does not offer detailed information on the formation of individual lipid droplets (LDs). Consequently, Raman imaging emerges as the preferred method for the molecular and morphological analysis of LDs in single endothelial and leukemic cells.

Spontaneous Raman Imaging

As demonstrated previously, infrared spectroscopy proves to be effective in studying the molecular structure of biological systems. However, this method encounters two primary limitations when applied to single-cell studies: low spatial resolution (on the order of microns) and high water absorption, making the investigation of cells *in vitro* under physiological conditions challenging or even impossible. Spectroscopic techniques based on Raman scattering have emerged to address these challenges.

Raman imaging enables label-free or labelled analysis of the buffered environment's cellular composition and metabolic changes. Due to the substantial cross-section for Raman scattering exhibited by lipids, this method is particularly elevant at tracking fatty acid uptake in individual cells [43-48]. Raman imaging overcomes the difficulties associated with infrared and fluorescent imaging, making it the technique of first choice for studying lipid metabolism in single cells under physiological conditions. Figure 3 shows representative Raman images of PA-d_{31}-treated (upper row) and control (bottom row) HMEC-1 (A) and HL-60 (B) cells.

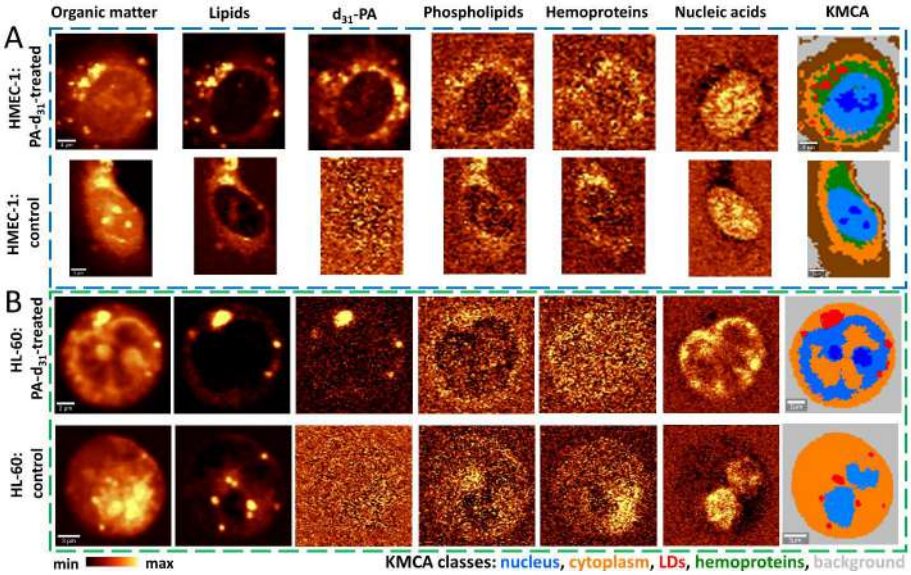

Fig 3. Raman imaging of PA-d_{31}-treated (upper row) and control (bottom row) HMEC-1 (A) (scale bar: 4 μm and 5 μm) and HL-60 (B) cells (scale bar: 2 μm and 3 μm). Raman distribution images of selected chemical components: organic matter (2830-3030 cm^{-1}), lipids (2830-2900 cm^{-1}), PA-d_{31} (2030-2230 cm^{-1}), phospholipids (705-735 cm^{-1}), hemoproteins (725-770 cm^{-1}), nucleus (775-805 cm^{-1}). KMCA shows the spatial distribution of subcellular components: cytoplasm and endoplasmic reticulum (brown, orange), nucleus (blue), LDs (red), hemoproteins (green), and background (grey).

It is possible to observe the spatial distribution of various biomolecules with high resolution using the full range of the Raman spectrum. This includes organic matter (3030-2830 cm^{-1}), lipids (2900-2830 cm^{-1}), PA-d_{31} (2230-2030 cm^{-1}), phospholipids (735-705 cm^{-1}), hemoproteins (770-725 cm^{-1}), and the nucleic acids (805-775 cm^{-1}) (Fig 3). It can be seen that newly formed LDs are located mainly near the lipid-rich perinuclear area and hemoproteins in cells. Furthermore, chemometric analysis, such as KMCA (K-Means Cluster Analysis), can be used to perform a multivariate analysis of Raman images, providing information about the distribution of the studied subcellular components, including LDs (marked in red), the nucleus (blue), and hemoproteins (green).

A significant advantage of Raman imaging is its ability for confocal imaging, which allows the visualization of subcellular composition and molecular changes throughout the cell volume [45,46].To demonstrate this advantage, Confocal Raman imaging was performed in depth along the cross-section of the cells (Figs 4 and 5 for endothelial and leukemic cells, respectively).

KMC analysis of Raman maps (for endothelial cells: Figure 4C and for leukemic cells: Figure 5C) allows for insight into the distribution of LDs within the cell (Fig 4E and 5E). Integration maps and KMCA results for the depth imaging of HMEC-1 and HL-60 cells show the distribution of the nucleus and newly

formed LDs. Confocal imaging in stack mode provides the three-dimensional distribution of the subcellular components. Figure 5F and Fig 5G show the distribution of the nucleus (blue) and LDs (red) throughout the volume of promyeloblastic cells. For clarity, the color of the cytoplasm has been converted to grey in the three-dimensional images.

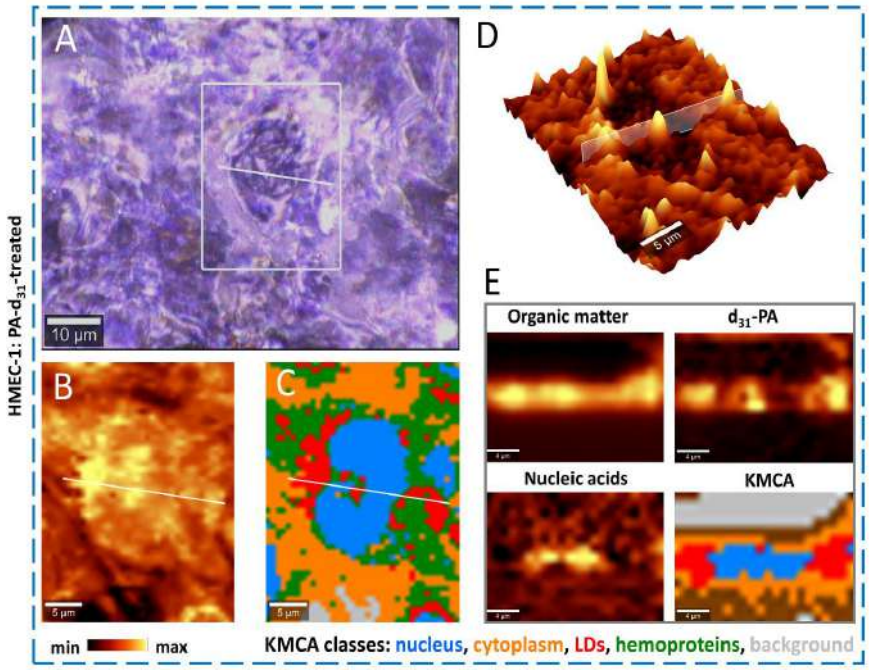

Fig 4. Confocal Raman imaging of PA-d_{31}-treated HMEC-1 cell: the whole cell with marked measured area (A), distribution of organic matter (an integration map over the 3030-2830 cm^{-1} range (scale bar 5 µm) (B), false-color KMCA image (C), distribution of PA-d_{31} (integration maps over the C-D stretching mode in 2200-2030 cm^{-1} range (scale bar 5 µm) (D), imaging of LDs in depth across the line marked in A-D of LDs (scale bar 4 µm) (E).

The presented results demonstrate the high applicability of Raman imaging in studies of metabolic alterations in single cells. Using Raman imaging, it is possible not only to visualize the spatial distribution of selected biomolecules, extended even to the entire cellular volume, but also to perform the simultaneous analysis of the structures of numerous cell biomolecules and the morphology of many subcellular components at the same time [45,48]. This dual capability improves the comprehensiveness of cellular studies, providing insights into both spatial and molecular aspects of cellular composition and metabolic changes.

Simulated Raman Spectroscopy

Although spontaneous Raman imaging offers numerous advantages, a significant drawback of this technique is the prolonged acquisition time for a single spectrum. This delay is attributed to the inherently low cross-section for Raman scattering of biomolecules in general [49].

In contemporary research efforts aimed at enhancing the efficiency of Raman imaging have focused on the development of nonlinear imaging techniques. One notable advancement in this domain is the emergence of Stimulated Raman Spectroscopy (SRS). SRS represents a cutting-edge approach beyond traditional linear Raman methods, offering improved signal generation and faster imaging capabilities. By leveraging nonlinearity, SRS addresses the inherent limitations of the low signal strength in spontaneous Raman scattering, thereby significantly enhancing the speed and sensitivity of Raman imaging processes.

This ongoing development holds promise for further advancement of the field and expansion of Raman spectroscopy applications in diverse scientific and technological domains [49]. The main advantages of SRS are the lack of a high fluorescence background, imaging speed (even 1 cell/s), and high confocality [49]. SRS and spontaneous Raman spectroscopy help to study LDs, but they have different limitations in terms of speed [32-35]. Figure 6 presents the acquired SRS images of HAEC and HL-60 cells at 2930 cm^{-1} (mainly proteins), 2850 cm^{-1} (mostly lipids), and 2100 cm^{-1} (the C-D stretching).

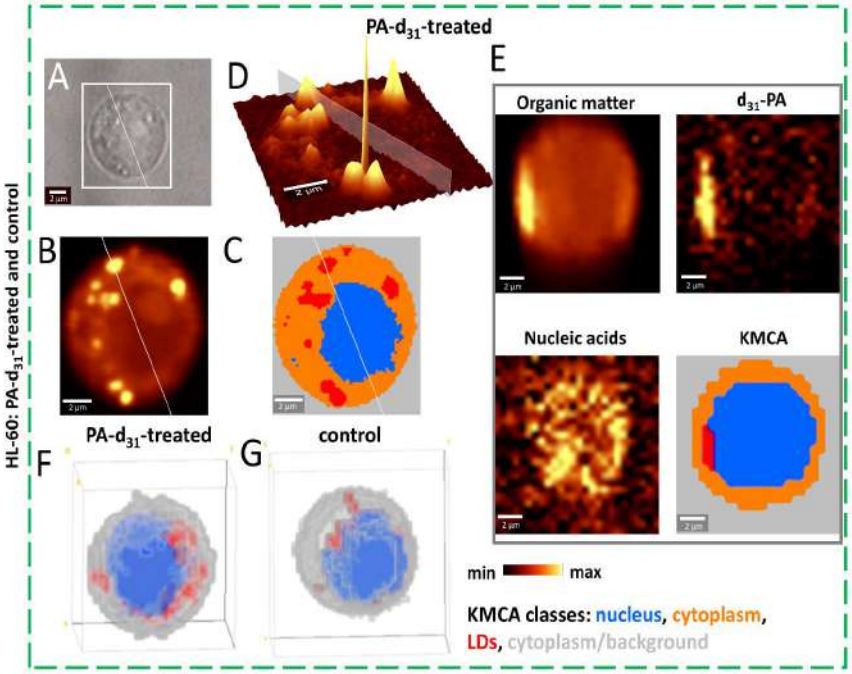

Fig 5. Confocal Raman imaging of PA-d_{31}-treated HL-60 cell: the whole cell with marked the measured area (A), distribution of organic matter (an integration map over the 3030-2830 cm^{-1} range) (B), false-color KMC image (C), distribution of PA-d_{31} (an integration maps over the C-D stretching mode in 2200-2030 cm^{-1} range (scale bar 2 µm) (D), imaging of LDs in depth across the line marked in A-C of LDs (scale bar 2 µm) (E), three-dimensional imaging of LDs (red) in PA-d_{31}-treated (F) and control (G) HL-60 cell. For clarity, the color of the cytoplasm has been converted to gray in the three-dimensional images.

The capability of detecting the SRS signal in a broad spectral range (1010 - 3615 cm^{-1}) enabled the generation of an SRS image focused on the distinctive signal of C-D vibrations in the PA-d_{31} molecules (2100 cm^{-1}). The acquired images vividly depict the spatial distribution of deuterated fatty acids, closely co-localizing with endogenous cellular lipids. These outcomes serve as compelling evidence that label-free spectroscopic imaging can surpass the effectiveness of fluorescent imaging when exploring metabolic changes in diverse cell types.

4 Conclusions

We conducted a comprehensive multiparameter spectroscopic analysis of lipid droplets (LDs) within individual endothelial cells, exemplified by two cell lines (HAEC and HMEC-1) and leukemic promyeloblasts, represented by HL-60 cells. This analysis was compared with conventional fluorescence staining methods. To specifically trace newly formed LDs due to fatty acid uptake and distinguish them from endogenous lipids, we utilized an exogenous deuterated palmitic acid (PA-d_{31}), characterized by a unique Raman band around 2100 cm^{-1} that does not overlap with other biomolecular vibrations.

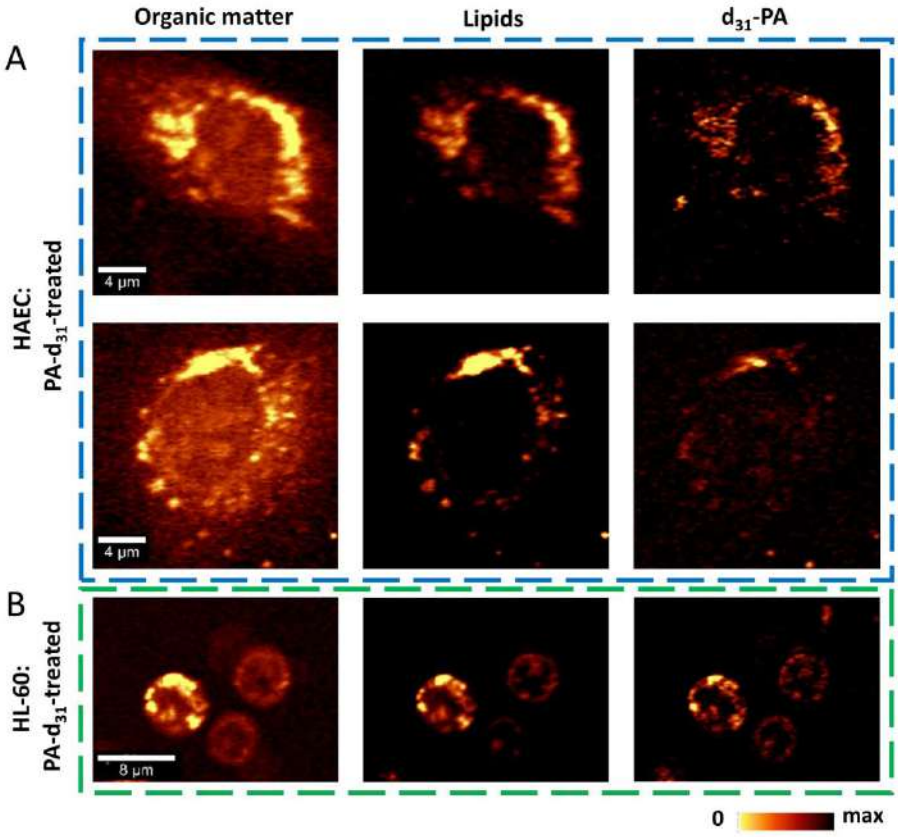

Fig 6. SRS images of HAEC (A) and HL-60 cells (B) incubated with d_{31}-PA from the left: organic matter (2930 cm^{-1}), lipids (2850 cm^{-1}), and d_{31}-PA (2100 cm^{-1}) (scale bar: 4 μm (for HAEC) and 8 μm (for HL-60)).

Infrared imaging proved to be effective in tracking deuterated fatty acid uptake in cells. However, its limitation lies in its poor spatial resolution, which makes studying the distribution of LDs at the single-cell level challenging and sometimes impossible. Additionally, infrared spectroscopy requires sample drying, which precludes studies under physiological conditions. On the contrary, spontaneous Raman imaging overcomes the limitations of infrared spectroscopy, but requires a relatively long imaging time (even several minutes *per* cell). On the other hand, stimulated Raman spectroscopy emerged to be the most efficient technique for studying the localization of LDs in cells, albeit with the constraint of recording signals for one wavenumber at a time.

Our research shows that spectroscopic methods are an excellent tool for studying LDs in single cells and provide comprehensive information that can complement studies conducted using classical techniques, such as fluorescence microscopy.

Acknowledgments

This article is based on a talk at the IX "International Conference on Perspectives in Vibrational Spectroscopy" (ICOPVS) at UGC-DAE Consortium for Scientific Research, Indore, Madhya Pradesh, India, by Dr Anna M Nowakowska that was awarded with the ***"Dayawati Rastogi Best Oral Presentation Award"*** by the Indian Spectroscopy Society and the Asian Journal of Physics on Dec 13, 2022.

Further, this work was partially supported by the National Science Centre (Poland) based on decision No. UMO-2016/21/D/ST4/00870. Authors would like to express gratitude to Mrs Karolina Augustyniak for assistance in FT-IR imaging measurements, Mr Kacper Siąkała for assistance in Raman imaging measurements, Mrs Adriana Adamczyk for help in cell culturing, and Prof Małgorzata Barańska for her unappreciated substantial support during the implementation of the study. This work was partially funded within the budget of the "Excellence Initiative - Research University" program at the Jagiellonian University in Krakow ("Young Laboratories" Program (Edition 2), "Real-time analysis of the metabolism of live cancer cells using stimulated Raman spectroscopy," no. WCh.1.5.2022.13).

References

1. Maekawa M, Fairn G D, Molecular probes to visualize the location, organization, and dynamics of lipids. *J Cell Sci*, 127(2014)4801–4812.
2. Olzmann J A, Carvalho P, Dynamics and functions of lipid droplets. *Nat Rev Mol Cell Biol*, 20(2019)137–155.
3. Majzner K, Chlopicki S, Baranska M, Lipid droplets formation in human endothelial cells in response to polyunsaturated fatty acids and 1-methyl-nicotinamide (MNA); confocal Raman imaging and fluorescence microscopy studies, *J Biophotonics*, 9(2016)396–405.
4. Murphy D J, Vance J, Mechanisms of lipid-body formation, *Trends Biochem Sci*, 24(1999)109–115.
5. Guo Y, Cordes K R, Farese R V, Walther T C, Lipid droplets at a glance, *J Cell Sci*, 122(2009)749–752.
6. Milger K, Herrmann T, Becker C, Gotthardt D, Zickwolf J, Ehehalt R, Watkins P A, Stremmel W, Füllekrug J, Cellular uptake of fatty acids driven by the ER-localized acyl-CoA synthetase FATP4, *J Cell Sci*, 119(2006)4678–4688.
7. Murphy S, Martin S, Parton R G, Lipid droplet-organelle interactions; sharing the fats, *Biochim Biophys Acta*, 1791(2009)441–447.
8. Ohsaki Y, Cheng J, Fujita A, Tokumoto T, Fujimoto T. Cytoplasmic lipid droplets are sites of convergence of proteasomal and autophagic degradation of apolipoprotein B, *Mol Biol Cell*, 17(2006)2674–2683.
9. Bagatolli L A, Gratton E, Two Photon Fluorescence Microscopy of Coexisting Lipid Domains in Giant Unilamellar Vesicles of Binary Phospholipid Mixtures, *Biophys J*, 78(2000)290–305.
10. Kuerschner L, Moessinger C, Thiele C, Imaging of lipid biosynthesis: how a neutral lipid enters lipid droplets, *Traffic*, 9(2008)338–352.
11. Vinegoni C, Botnaru I, Aikawa E, Calfon M A, Iwamoto Y, Folco E J, Ntziachristos V, Weissleder R, Libby P, Jaffer F A, Indocyanine Green Enables Near-Infrared Fluorescence Imaging of Lipid-Rich, Inflamed Atherosclerotic Plaques, *Sci Transl Med*, 3(2011)84ra45, doi:10.1126/scitranslmed.3001577.
12. Zheng X, Zhu W, Ni F, Ai H, Yang C, A specific bioprobe for super-resolution fluorescence imaging of lipid droplets, *Sensors Actuators B Chem*, 255(2018)3148–3154.
13. Listenberger L L, Studer A M, Brown D A, Wolins N E, Fluorescent detection of lipid droplets and associated proteins, *Curr Protoc Cell Biol*, 2016;71:4.31.1-4.31.14; doi:10.1002/cpcb.7.
14. Ohsaki Y, Shinohara Y, Suzuki M, Fujimoto T, A pitfall in using BODIPY dyes to label lipid droplets for fluorescence microscopy, *Histochem Cell Biol*, 133(2010)477–480; doi:10.1007/s00418-010-0678-x.
15. Greenspan P, Mayer E P, Fowler S D, Nile red: A selective fluorescent stain for intracellular lipid droplets, *J Cell Biol*, 100(1985)965–973; doi:10.1083/jcb.100.3.965.
16. DiDonato D, Brasaemle D L, Fixation methods for the study of lipid droplets by immunofluorescence microscopy, *J Histochem Cytochem*, 51(2003)773–780.
17. Astanina K, Koch M, Jüngst C, Zumbusch A, Kiemer A K, Lipid droplets as a novel cargo of tunnelling nanotubes in endothelial cells, *Sci Rep*, 5(2015)1–13.
18. Toman K, What are the disadvantages and disadvantages of fluorescence microscopy, In: Frieden T, ed. *Toman's Tuberculosis Case Detection, Treatment, and Monitoring – Questions and Answers*, 2nd edn, (World Health Organization), 2004, pp 31–34.

19. Ami D, Posteri R, Mereghetti P, Porro D, Doglia S M, Branduardi P, Fourier transform infrared spectroscopy as a method to study lipid accumulation in oleaginous yeasts, *Biotechnol Biofuels*, 7(2014):1-14; doi:10.1186/1754-6834-7-12.
20. Kodali D R, Small D M, Powell J, Krishnan K, Infrared Micro-Imaging of Atherosclerotic Arteries, *Appl Spectrosc*, 45(1991)1310–1317.
21. Czamara K, Majzner K, Pacia M Z, Kochan K, Kaczor A, Baranska M, Raman spectroscopy of lipids: a review. *J Raman Spectrosc*, 46(2015)4–20.
22. Freudiger C W, Min W, Saar B G, Lu S, Holtom G R, He C, Tsai J C, Kang J X, Xie X S, Label-Free Biomedical Imaging with High Sensitivity by Stimulated Raman Scattering Microscopy, *Science*, 322(2008)1857–1861.
23. Kochan K, Maslak E, Krafft C, Kostogrys R, Chlopicki S, Baranska M, Raman spectroscopy analysis of lipid droplets content, distribution and saturation level in Non-Alcoholic Fatty Liver Disease in mice, *J Biophotonics*, 8(2015)597–609.
24. Tirinato L, Liberale C, Di Franco S, Candeloro P, Benfante A, Rocca R L, Potze L, Marotta R, Ruffilli R, Rajamanickam V P, Malerba M, Angelis F D, Falqui A, Carbone E, Todaro M, Medema J P, Stassi G, Fabrizio E D, Lipid droplets: A new player in colorectal cancer stem cells unveiled by spectroscopic imaging, *Stem Cells*, 33(2015)35–44.
25. Jaeger D, Pilger C, Hachmeister H, Oberländer E, Wördenweber R, Wichmann J, Mussgnug J H, Huser T, Kruse O, Label-free *in vivo* analysis of intracellular lipid droplets in the oleaginous microalga Monoraphidium neglectum by coherent Raman scattering microscopy, *Sci Rep*, 6(2016)35340; doi:10.1038/srep35340.
26. Baena J R, Lendl B, Raman spectroscopy in chemical bioanalysis, *Curr Opin Chem Biol*, 8(2004)534–539.
27. He XN, Allen J, Black PN, T Baldacchini, X Huang, H Huang, L Jiang, YF Lu, Coherent anti-Stokes Raman scattering and spontaneous Raman spectroscopy and microscopy of microalgae with nitrogen depletion, *Biomed Opt Express*, 3(2012)2896; doi:10.1364/boe.3.002896
28. Ferrara M A, Filograna A, Ranjan R, Corda D, Valente C, Sirleto L, Three-dimensional label-free imaging throughout adipocyte differentiation by stimulated Raman microscopy, *PLoS One*, 14(2019)e02196811; doi:10.1371/journal.pone.0216811
29. Zhang C, Li J, Lan L, Cheng J X, Quantification of Lipid Metabolism in Living Cells through the Dynamics of Lipid Droplets Measured by Stimulated Raman Scattering Imaging, *Anal Chem*, 89(2017)4502–4507.
30. Huang K C, Li J, Zhang C, Tan Y, Cheng J X, Multiplex Stimulated Raman Scattering Imaging Cytometry Reveals Lipid-Rich Protrusions in Cancer Cells under Stress Condition. *iScience*, 23(2020)100953; doi:10.1016/j.isci.2020.100953.
31. Jia H, Yue S, Stimulated Raman Scattering Imaging Sheds New Light on Lipid Droplet Biology, *J Phys Chem B*, 127(2023)2381–2394.
32. Tatenaka Y, Kato H, Ishiyama M, Sasamoto K, Shiga M, Nishitoh H, Ueno Y, Monitoring Lipid Droplet Dynamics in Living Cells by Using Fluorescent Probes, *Biochemistry*, 58(2019)499–503.
33. Zhao Y, Shi W, Li X, Ma H, Recent advances in fluorescent probes for lipid droplets, *Chem Commun*, 58(2022)1495–1509.
34. Neher R, Neher E, Optimizing imaging parameters for the separation of multiple labels in a fluorescence image, *J Microsc*, 213(2004)46–62.
35. Jensen E C, Use of Fluorescent Probes: Their Effect on Cell Biology and Limitations, *Anat Rec*, 295(2012)2031–2036.
36. Marzec K M, Rygula A, Gasior-Glogowska M, Kochan K, Czamara K, Bulat K, Malek K, Kaczor A, Baranska M, Vascular diseases investigated *ex vivo* by using Raman, FT-IR and complementary methods, *Pharmacol Reports*, 67(2015)744–750.
37. Chrabaszcz K, Kochan K, Fedorowicz A, Jasztal A, Buczek E, Leslie L S, Bhargava R, Malek K, Chlopicki S, Marzec K M, FT-IR- and Raman-based biochemical profiling of the early stage of pulmonary metastasis of breast cancer in mice, *Analyst*, 143(2018)2042–2050.

38. Blat A, Dybas J, Chrabaszcz K, Bulat K, Jasztal A, Kaczmarska M, Pulyk R, Popiela T, Slowik A, Malek K, Adamski M G, Katarzyna M, FTIR, Raman and AFM characterization of the clinically valid biochemical parameters of the thrombi in acute ischemic stroke, *Sci Rep*, 9(2019)15475; doi:10.1038/s41598-019-51932-0.
39. Chrabaszcz K, Jasztal A, Smęda M, Zieliński B, Blat A, Diem M, Chlopicki S, Malek K, Marzec K M, Label-free FTIR spectroscopy detects and visualizes the early stage of pulmonary micrometastasis seeded from breast carcinoma. *Biochim Biophys Acta - Mol Basis Dis*, 1864 (2018)3574–3584.
40. Kochan K, Kus E, Szafraniec E, Wislocka A, Chlopicki S, Baranska M, Changes induced by non-alcoholic fatty liver disease in liver sinusoidal endothelial cells and hepatocytes: Spectroscopic imaging of single live cells at the subcellular level, *Analyst*, 142(2017)3948–3958.
41. Wiercigroch E, Staniszewska-Slezak E, Szkaradek K, Wojcik T, Ozaki Y, Baranska M, Malek K, FT-IR Spectroscopic Imaging of Endothelial Cells Response to Tumor Necrosis Factor-α: To Follow Markers of Inflammation Using Standard and High-Magnification Resolution, *Anal Chem*, 90(2018)3727–3736.
42. Majzner K, Kochan K, Kachamakova-Trojanowska N, Maslak E, Chlopicki S, Baranska M, Raman imaging providing insights into chemical composition of lipid droplets of different size and origin: In hepatocytes and endothelium, *Anal Chem*, 86(2014)6666–6674.
43. Czamara K, Majzner K, Pacia M Z, Kochan K, Kaczor A, Baranska M, Raman spectroscopy of lipids: A review. *J Raman Spectrosc*, 46(2015)4–20.
44. Szafraniec E, Kus E, Wislocka A, Kukla B, Sierka E, Untereiner V, Sockalingum GD, Chlopicki S, Baranska M, Raman spectroscopy–based insight into lipid droplets presence and contents in liver sinusoidal endothelial cells and hepatocytes, *J Biophotonics*, 12(2019); doi:10.1002/jbio.201800290.
45. Bik E, Ishigaki M, Blat A, Jasztal A, Ozaki Y, Malek K, Baranska M. Lipid droplet composition varies based on medaka fish eggs development as revealed by NIR-, MiR-, and Raman imaging, *Molecules*, 25(2020)817; doi:10.3390/molecules25040817.
46. Majzner K, Chlopicki S, Baranska M, Lipid droplets formation in human endothelial cells in response to polyunsaturated fatty acids and 1-methyl-nicotinamide (MNA); confocal Raman imaging and fluorescence microscopy studies, *J Biophotonics*, 9(2016)396–405.
47. Czamara K, Majzner K, Selmi A, Baranska M, Ozaki Y, Kaczor A, Unsaturated lipid bodies as a hallmark of inflammation studied by Raman 2D and 3D microscopy, *Sci Rep*, 7(2017)40889; doi.10.1038/srep40889.
48. Borek-Dorosz A, Nowakowska A M, Leszczenko P, Adamczyk A, Pieczara A, Jakubowska J, Pastorczak A, Ostrowska K, Ząbczyńska M, Sowinski K, Gruszecki W I, Baranska M, Marzec K M, Majzner K, Raman-based spectrophenotyping of the most important cells of the immune system, *J Adv Res*, 41(2022)191–203.
49. Brzozowski K, Matuszyk E, Pieczara A, Firlej J, Nowakowska A M, Baranska M, Stimulated Raman Scattering Microscopy in Chemistry and Life Science – Development, Innovation, Perspectives, *Biotechnol Adv*, 60(2022) 108003; doi.org/10.1016/j.biotechadv.2022.108003.

[*Received*: 28.02.2024]

Anna M Nowakowska is an Assistant Professor at the Raman Imaging Group, Faculty of Chemistry, Jagiellonian University, Krakow. She completed her Ph.D. with honors in 2019 from the Henryk Niewodniczanski Institute of Nuclear Physics, Polish Academy of Science in Krakow. Her research focuses on biological systems using infrared and Raman spectroscopy and nanospectroscopy. As a part of her doctoral dissertation, Anna studied chromatin using AFM-IR and TERS nanospectroscopy. Currently, Anna conducts research aimed at the identification of spectral markers of leukemic cells using Raman spectroscopy and chemometric methods in the context of the clinical diagnosis of hematopoietic

malignancies. Anna worked in several projects, both national and international, completed research internships in Japan (Osaka University), USA (Columbia University), Switzerland (ETH Zurich), France (Université Bordeaux), published 20 papers and book chapters (e.g. TrAC Trends in Analytical Chemistry 2023, Biotechnology Advances 2022, Journal of Advanced Research 2022, Nucleic Acids Research 2019), she has been supervising several master and bachelor theses, is co-author of three patent applications, and gave invited lecture at International Conference on Perspectives in Vibrational Spectroscopy 2022, Indore, India, and invited talk at RSC Molecular Spectroscopy Group Online Seminar Series 2021 and 1st European Forum on Nanoscale Spectroscopy 2016.

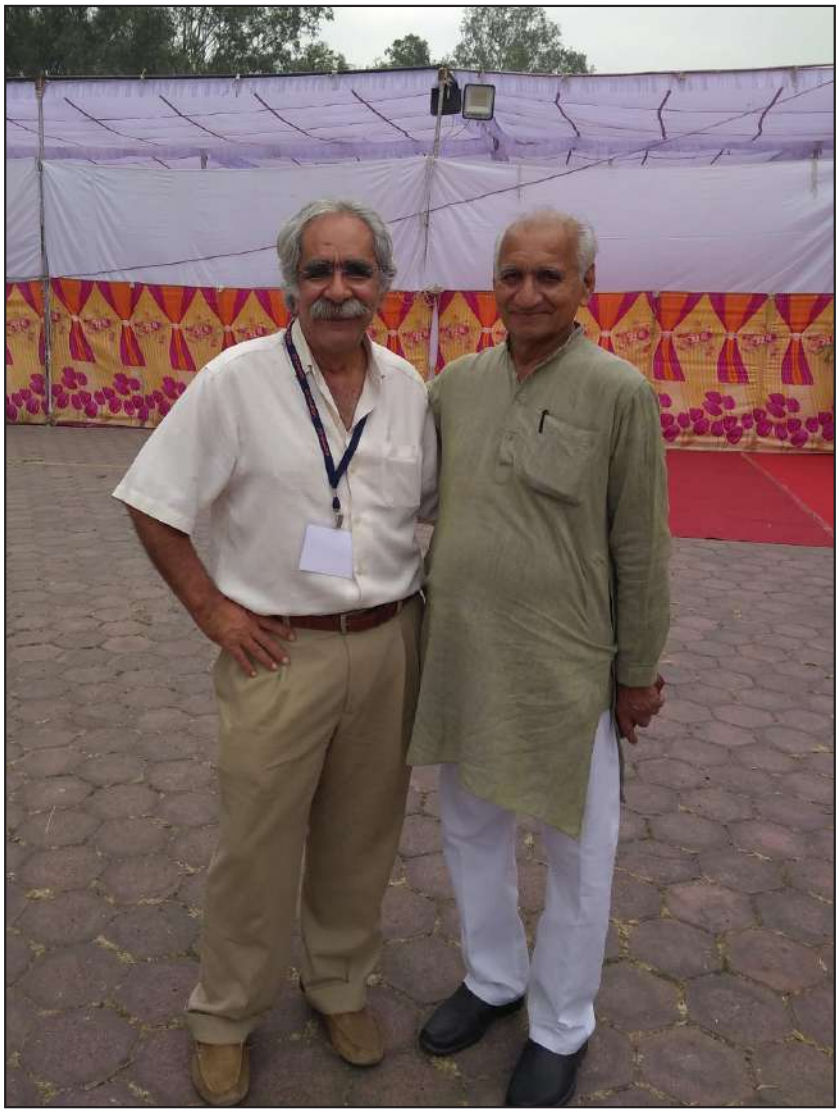

Photo: Vinod Rastogi (right), and V Apkarian(left) during IX ICOPVS 2022 on Dec 13,2022, Indore, India.

Photo:Vinod Rastogi (left), Shiva Umapathy (right) during IX ICOPVS 2022, Indore on Dec 13,2022

Photo: (from L to R) Anna Nowakowska, Laxmi, V Apkarian, Katarzyna Majzner (Dayawati Rastogi Lecture Awardee 2022), Vinod Rastogi (Founder of series of ICOPVS Conferences), during IX ICOPVS 2022, on Dec 16, 2022, Indore, India.